American Mineralogist, Volume 84, pages 55–69, 1999

Chemistry and genetic implications of tourmaline and Li-F-Cs micas from the Valdeflores area (Cáceres, Spain)

Alfonso Pesquera,[1,*] Jose Torres-Ruiz,[2] Pedro P. Gil-Crespo,[1] and Nicolas Velilla[2]

[1]Departamento de Mineralogía y Petrología, Universidad del país Vasco 644, 48080 Bilbao, Spain
[2]Departamento de Mineralogía y Petrología, Universidad de Granada, E-18002 Granada, Spain

Abstract

Pervasive metasomatism that involved the formation of tourmaline-rich rocks and influx of Li, F, and Cs into Ordovician psammo-pelitic metasediments occurred in the Valdeflores area (Cáceres, Spain). Numerous Li- and Sn-bearing, mineralized, greisen-type veins also can be observed here, in the vicinity of geochemically specialized granites. Tourmaline-rich rocks appear as: (1) massive, fine-grained, dark green to black rocks; and (2) fine-scale tourmaline-rich laminae, which alternate with quartz-rich layers parallel to the bedding.

Electron microprobe analyses indicate that the tourmaline lies mostly within the space defined by the exchange vectors from dravite: $FeMg_{-1}$ (schorl), $\square AlNa_{-1}Mg_{-1}$ (foitite), $AlOMg_{-1}(OH)_{-1}$ (olenite), and $CaMgNa_{-1}Al_{-1}$ (uvite). The Fe/(Fe+Mg) ratio ranges mainly from 0.87 to 0.54 and increases with Al in the Y-site. Analytical results and substitutional relations show an insignificant elbaite component. Mica in the tourmalinized rocks is very fine-grained (mostly <50 μm). White mica ranges from lithian muscovite-phengite to lepidolite/zinnwaldite, containing up to 8.40 wt% F, 6.0 wt% Li_2O, and 10.73 wt% FeO. Dark mica shows a variable color and has compositions characterized by relatively high contents of Cs_2O (1.14–2.78 wt%) and F (1.94–8.08 wt%), with a deficit in K_2O (5.75–9.04 wt%). Log (f_{H_2O}/f_{HF}) of fluids in equilibrium with biotite in the tourmaline-rich rocks was 4.02–4.17 at $T \approx 400$ °C. Log (f_{H_2O}/f_{HF}) values of fluids in equilibrium with topaz ($X_F \approx 0.8$) in country rock adjacent to contacts with veins, and in equilibrium with amblygonite-montebrasite ($X_{amb} = 0.2$) in the veins were about 4.30–4.60 and 6.4–6.7, respectively. These variations denote the existence of gradients in relative a_{HF} more than differences of temperature during metasomatism. The lack of tourmaline in the veins is interpreted to reflect the alkalinity and low Fe-Mg contents in the fluids, which precluded the formation of tourmaline. Consequently, most of the boron was expelled into metasediments where tourmaline was produced as a result.

Introduction

The Valdeflores area is located in the Central-Iberian zone, near Cáceres, Spain (Fig. 1). In this region, three lithologic assemblages can be distinguished: (1) Precambrian metasedimentary rocks (Schist-Graywacke Complex); (2) a Paleozoic sequence composed of quartzite, sandstone, and pelite, with subordinate volcanic tuff and carbonate rock, forming part of the Cáceres syncline; and (3) metallogenically specialized granites of calc-alkaline to alkaline character. The metasedimentary rocks record the effects of three periods of Hercynian deformation including folding and shearing, and a low-grade regional metamorphism that developed during D1 deformation (López Plaza and Martínez Catalán 1988).

Tourmaline-rich rocks occur in Ordovician psammo-pelitic metasediments of the Valdeflores area (Fig. 2), near the eastern margin of the Cabeza de Araya batholith and close to small bodies of tectonized granite. Tourmaline-rich rocks are outside the thermal aureole of these granites, and cover a NE-SW trending elliptical area of approximately 250 × 500 m. Drilling has revealed that the tourmaline-rich rocks extend to depths of at least 350 m. A set of quartz- and greisen-type veins is spatially associated with the tourmaline-rich rocks. These veins strike mainly NE–SW, dip subvertically to the NW, and cut the regional foliation at very high angle. However, a systematic variation in the modal volume of tourmaline with distance from veins is not observed. Field and petrographic data are consistent with an epigenetic origin for the tourmaline-rich rocks (Torres-Ruiz et al. 1996). These rocks contain up to 80% tourmaline by volume, with the remainder being Li-F-Cs mica, quartz, topaz, and arsenopyrite. This mineral association is believed to be the result of the interaction between B, F, and alkali-rich magmatic-hydrothermal fluids and psammo-pelitic metasediments. Similar examples where tourmaline and Li-F-Cs

* E-mail: npppepea@lg.ehu.es

0003–004X/99/0102–0055$05.00

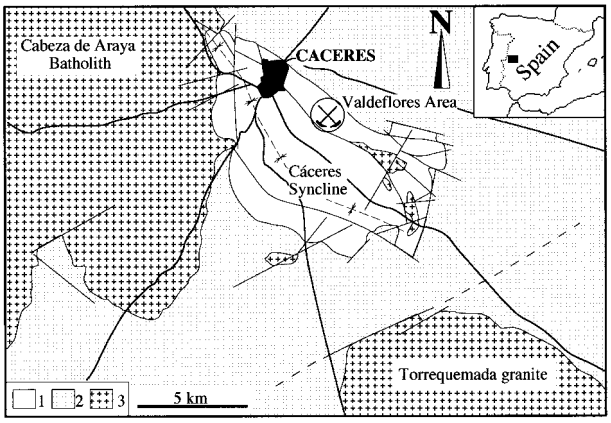

FIGURE 1. Location of the Valdeflores area. (1) Paleozoic rocks of the ''Cáceres syncline.'' (2) Precambrian rocks of the ''Schist-Graywacke Complex.'' (3) Granitic rocks.

micas are the products of metasomatic alteration have been described by other workers (e.g., Glebov et al. 1974; Morgan and London 1987).

This paper reports on the mineral paragenesis and chemistry of tourmaline and associated micas, and discusses their significance in deciphering the nature of metasomatic processes. Interest in tourmaline as a recorder of crystallization history and environment of formation is well documented (e.g., Henry and Guidotti 1985; Jollif et al. 1986; Gallagher and Kennan 1992; London and Manning 1995; Henry and Dutrow 1996; London et al. 1996; Slack 1996). Likewise, in granite-hydrothermal systems, the micas have been used as markers of chemical fractionation and petrogenetic indicators, as well as for characterizing relative HF, HCl, O_2, and H_2O fugacities in the fluids (e.g., Černý and Burt 1984; Munoz 1984; Jollif et al. 1987; van Middelaar and Keith 1990; Lentz 1992; Hecht 1994; Foord et al. 1995; Roda et al. 1995; Finch et al. 1995; Stone et al. 1997).

ANALYTICAL METHODS

Mineral compositions were determined with a Cameca SX50 electron microprobe at the University of Granada, equipped with four wavelength-dispersive spectrometers, using both natural and synthetic standards: natural fluorite (F), natural sanidine (K), natural pollucite (Cs), synthetic $MnTiO_3$ (Ti, Mn), natural diopside (Ca), synthetic $BaSO_4$ (Ba), synthetic Fe_2O_3 (Fe), natural albite (Na), natural periclase (Mg), synthetic SiO_2 (Si), natural apatite (P), and synthetic Al_2O_3 (Al). An accelerating voltage of 20 kV, with a beam current of 30 nA and a beam diameter of about 1 μm, were used to analyze tourmaline and micas. The counting times on peak were twice those of background, with 15 s for Na and K; 20 s for Ti, Ca, P, and Ba; 25 s for Fe, Si, and Al and 30 s for Cs and Mg. Phosphates were analyzed at 20 kV, with a 20 nA beam current and 5 μm spot size. F was determined by measurement of the integrated peak area in the total range from 0.015 to 0.0450 sin θ for silicates and phosphates,

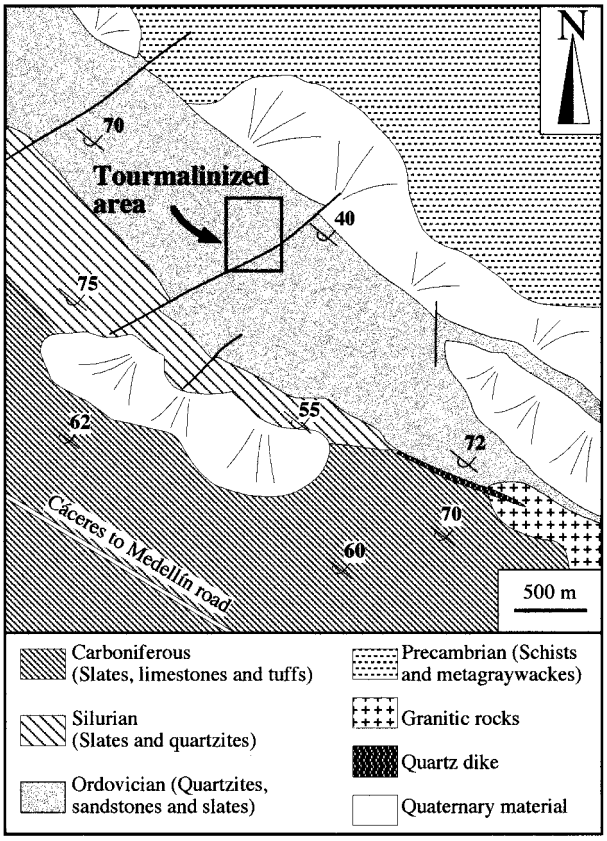

FIGURE 2. Geology of the Valdeflores area.

respectively, both in the standard and in the sample. Data were reduced using the procedure of Pouchou and Pichoir (1985). Structural formulae of micas have been calculated on the basis of 11 O atoms in accord with the models discussed by Loucks (1991).

Li in tourmaline and mica separates was analyzed at the University of Granada using an inductively coupled plasma mass spectrometry (ICP-MS) technique with Perkin Elmer SCIEX Elan-5000 equipment. Representative white mica separates were also examined by X-ray diffraction (XRD), by Raman and Fourier-transform infrared spectroscopies (FTIR), and by thermogravimetric analyses (TGA). Mica polytypes were identified from XRD patterns recorded on a Phillips PW1729 instrument ($CuK\alpha_1$ = 1.5406 Å), using the data of Bailey (1984). Two scans (step interval = 0.02°θ, exposure time = 2.5 s) were made for each sample.

IR data were recorded at room temperature with a Nicolet-740 FTIR spectrometer, using 0.1 mg of sample as KBr pellets (total weight = 50 mg) in the spectral region 4000–400 cm^{-1}. The scanning conditions were 1 cm^{-1} nominal resolution, normal Beer-Norton apodization function, and 0.2 cm^{-1}/s scan speed. Raman spectra were recorded at room temperature on a Nicolet 950 FT Raman spectrometer equipped with a Spectra Physics Nd:YVO_4 laser (1064 nm, 1.5 W). The uncertainty on peak posi-

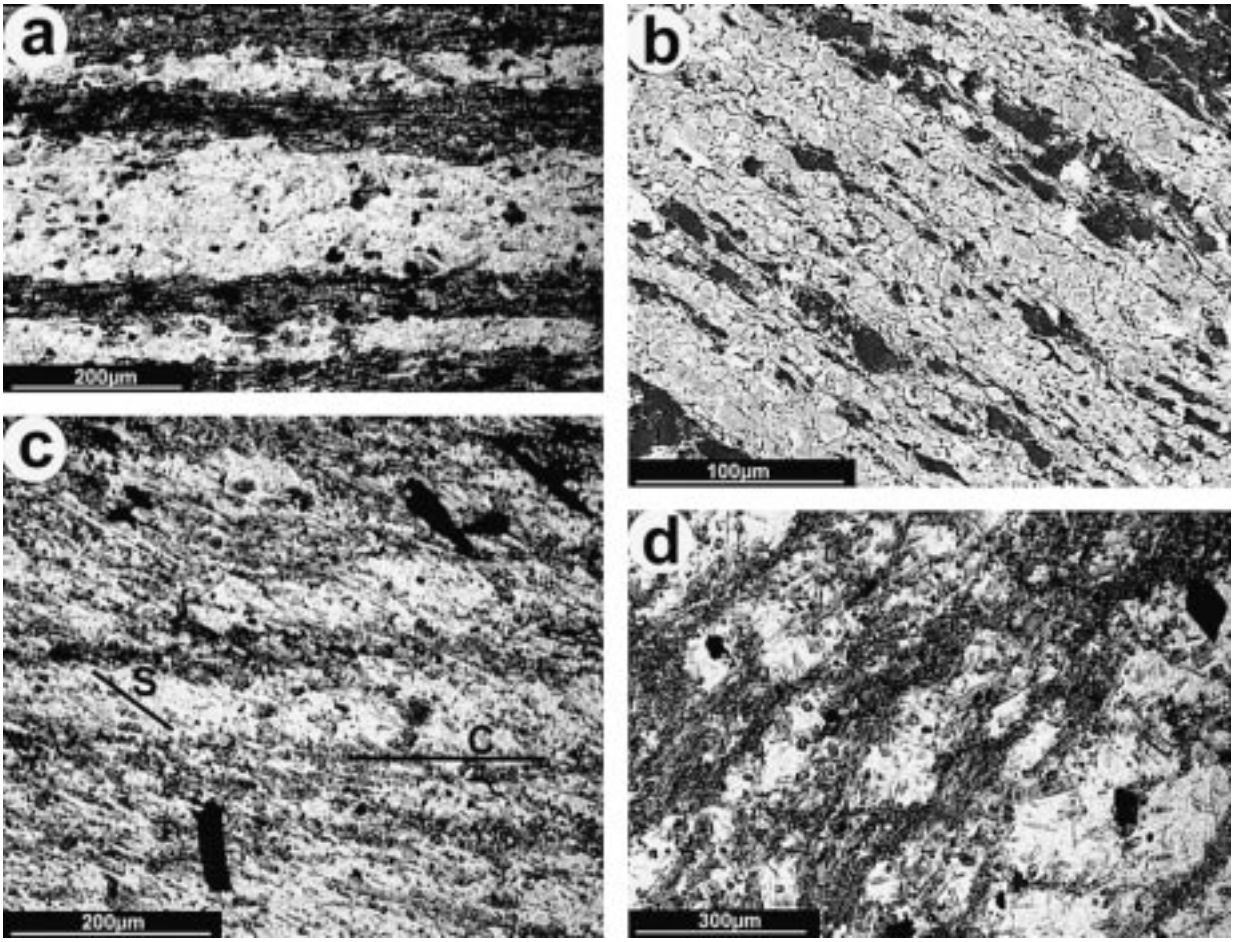

FIGURE 3. Representative tourmaline-rich rocks from the Valdeflores area. **(a)** Photomicrograph of laminated tourmaline-rich rock in which fine-grained tourmaline laminae alternate with quartz- and mica-rich laminae. (**b**) Backscattered electron image of banded tourmalinite in which tourmaline and quartz correspond to the light gray and dark gray bands, respectively. (**c**) Photomicrograph showing S-C microstructures in tourmaline-rich rock. (**d**) Photomicrograph showing porphyroclastic texture in which quartz-mica augen clasts are wrapped by fine-grained tourmaline crystals.

tions is ± 2 cm^{-1} for high-intensity bands, and at least two times greater for low-intensity bands and shoulders. Variations of OH-stretching Raman band intensities have been used to evaluate the F-OH content. The band intensities have been normalized by comparison with the high-intensity band assigned to the symmetric Si-O-Si vibration ($\approx$700 cm^{-1}) that is used as an internal intensity standard (Robert et al. 1993). A Setaram TAG 24S 16 thermobalance was used to obtain the differential thermal analysis (DTA) and thermogravimetric analysis (TGA) curves simultaneously, in a synthetic air atmosphere and in an inert atmosphere of argon. The heating rate was 10°/min for all samples, and 14–16 mg of mica were used for each analysis. Analysis of F in the solid residue revealed that no detectable amount of F was lost during thermal analysis. It was not possible to separate dark micas from the rocks for spectroscopic analysis due to their very fine-grain size, low abundance, and irregular distribution.

PETOGRAPHY

Tourmaline is an accessory detrital mineral in Ordovician metasediments of the Cáceres syncline, in which it is fine-grained and shows variable rounding and color. In tourmaline-rich rocks from the Valdeflores area, however, tourmaline appears as: (1) fine-scale laminations, where laminae of fine-grained tourmaline alternate with quartz- and mica-rich laminae (Figs. 3a and 3b); (2) poorly or randomly oriented crystals disseminated in a very fine-grained quartz-mica matrix; (3) more or less elongated lenticular aggregates parallel to bedding; (4) concentrations along S-C deformation planes (Fig. 3c); and (5) a matrix for porphyroclastic, lozenge-shaped, quartz-mica fragments (Fig. 3d). White mica, dark mica, and quartz are the main associated silicates. Country rocks adjacent to contacts with greisen-type veins are locally spotted by small ($<$250 µm) topaz poikiloblasts. Opaque minerals include arsenopyrite, particularly in

TABLE 1. Representative microprobe analyses of tourmaline

Sample	1	2	3	4	5	6	7
SiO_2	36.94	36.14	36.69	36.08	36.28	36.62	36.43
TiO_2	0.55	0.63	0.45	0.79	0.59	0.63	0.57
Al_2O_3	32.67	32.63	33.21	31.85	31.65	32.55	32.63
FeO_{tot}	9.97	10.14	11.85	10.71	10.98	11.34	13.06
MnO	0.04	0.03	0.03	0.03	0.00	0.08	0.07
MgO	4.18	4.32	2.40	4.19	4.36	3.20	1.92
CaO	0.66	1.21	0.09	0.92	1.21	0.14	0.08
Na_2O	1.74	1.63	2.22	1.66	1.62	2.26	2.30
K_2O	0.12	0.05	0.03	0.06	0.05	0.03	0.04
F	0.53	0.60	0.85	0.54	0.60	1.05	1.34
O = F	0.22	0.25	0.36	0.23	0.25	0.44	0.56
	87.18	87.13	87.47	86.61	87.09	87.46	87.89
H_2O*	3.02	2.900	2.43	3.03	2.90	2.07	1.54
B_2O_3*	10.67	10.63	10.64	10.53	10.57	10.65	10.62
Total	100.87	100.66	100.54	100.17	100.56	100.16	100.03
Structural formula on the basis of 24.5 O atoms							
Si	6.017	5.913	5.996	5.957	5.968	5.978	5.961
$^{[4]}$Al	0.000	0.087	0.004	0.043	0.032	0.022	0.039
B	3.000	3.000	3.000	3.000	3.000	3.000	3.000
Al(Z)	6.000	6.000	6.000	6.000	6.000	6.000	6.000
Al(Y)	0.274	0.207	0.394	0.156	0.105	0.242	0.256
Ti	0.068	0.078	0.055	0.099	0.073	0.078	0.070
Fe^{2+}	1.359	1.388	1.619	1.479	1.510	1.548	1.787
Mn	0.005	0.005	0.005	0.005	0.000	0.011	0.011
Mg	1.016	1.054	0.586	1.031	1.069	0.778	0.467
Y total	2.722	2.732	2.659	2.770	2.757	2.657	2.591
Ca	0.115	0.211	0.016	0.163	0.213	0.025	0.014
Na	0.551	0.518	0.703	0.532	0.516	0.716	0.731
K	0.024	0.010	0.007	0.013	0.011	0.006	0.009
X total	0.690	0.739	0.726	0.708	0.740	0.747	0.754
F	0.274	0.312	0.441	0.280	0.314	0.543	0.693
OH	3.726	3.688	3.559	3.720	3.686	3.457	3.307
Fe/(Fe + Mg)	0.57	0.57	0.73	0.59	0.59	0.67	0.79
Na/(Na + Ca)	0.83	0.71	0.98	0.77	0.71	0.97	0.98

* Calculated.

zones near veins. Zircon, apatite, and rutile are accessories.

Tourmaline shows euhedral to subhedral prismatic habit, is fine- to very fine-grained (500–20 μm) and, in thin section, is bluish-green or green to yellowish brown. Some crystals display a slightly pronounced, gradational to discontinuous optical zoning, with green cores and pale green rims.

White mica is dominant relative to dark mica, and both occur in two ways: (1) as fine to very fine-grained prismatic crystals (<150 μm) oriented along the foliation of the rocks; and (2) as ultrafine to very fine-grained crystals (mostly <50 μm), disseminated and randomly orientated in the rocks. The latter petrographic type is more abundant. The randomly oriented white micas locally exhibit greenish, yellowish, or pinkish hues. Dark mica displays variable color: pale gray, green, or orange to pinkish brown, with a relatively low birefringence (<0.030). Yellowish- to reddish-brown biotite with high birefringence (>0.040) also has been observed in places, both randomly oriented and along foliation planes in the rocks. This kind of biotite is believed to be representative of biotite that developed during thermal metamorphism, prior to the metasomatic processes, because it occurs locally in untourmalinized country rocks. In contrast, the variable-colored biotite, with lower birefringence and different composition, is of metasomatic origin. Some mica grains exhibit an irregular color zonation where biotite is surrounded by white mica. In general, the coexistence at the grain scale of both types of micas is relatively common.

In the mineralized veins spatially associated with tourmalinites, white mica coexists with quartz, apatite, amblygonite-montebrasite, cassiterite, fluorite, topaz, and potassium feldspar, and appears as: (1) palm-like or comb-structured crystals (<1 cm); and (2) very-fine to ultrafine-grained crystals (<30 μm) replacing preexisting minerals and forming massive bodies near the coarse-grained quartz.

TOURMALINE CHEMISTRY

Tourmaline has a general formula that can be written $XY_3Z_6(BO_3)_3T_6O_{18}W_4$, for which X = Na, Ca, K, vacancy (□); Y = Mg, Fe^{2+}, Fe^{3+}, Li, Al, Mn, Ti^{4+}, Cr^{3+}; Z = Al, Mg, Fe^{3+}, Cr^{3+}; T = Si, Al; W = OH^-, F^-, O^{2-} (Hawthorne 1996). The crystal chemistry of tourmaline nevertheless is very difficult to characterize fully because some significant components (e.g., Li, Fe^{3+}, H_2O) cannot be determined by electron microprobe analysis. Likewise,

TABLE 1—*Extended*

8	9	10	11	12	13	14	15
36.67	36.35	36.23	36.32	36.77	36.07	36.63	36.75
0.52	0.52	0.6	0.63	0.55	0.79	0.58	0.44
32.25	32.37	32.23	31.73	32.2	31.09	33.22	33.72
12.69	12.81	13.37	13.03	13.45	11.5	9.59	9.38
0.03	0.09	0.06	0.07	0.08	0.02	0.05	0.03
2.84	2.01	2.13	2.67	1.92	3.84	4.29	4.37
0.09	0.35	0.07	0.07	0.06	0.35	0.64	0.48
2.33	2.14	2.32	2.38	2.28	2.29	1.8	1.79
0.04	0.08	0.05	0.06	0.04	0.05	0.03	0.03
0.91	1.00	1.00	1.05	1.13	0.92	0.28	0.25
0.38	0.42	0.42	0.44	0.47	0.39	0.12	0.11
87.98	87.3	87.65	87.55	88.01	86.52	86.98	87.14
2.34	2.18	2.18	2.09	1.94	2.34	3.49	3.53
10.63	10.54	10.55	10.55	10.61	10.48	10.66	10.70
100.95	99.99	100.35	100.19	100.56	99.35	101.13	101.38
Structural formula on the basis of 24.5 O atoms							
5.996	5.994	5.968	5.984	6.024	5.982	5.974	5.969
0.004	0.006	0.032	0.016	0.000	0.018	0.026	0.031
3.000	3.000	3.000	3.000	3.000	3.000	3.000	3.000
6.000	6.000	6.000	6.000	6.000	6.000	6.000	6.000
0.213	0.286	0.229	0.147	0.217	0.061	0.361	0.425
0.064	0.065	0.074	0.078	0.068	0.098	0.071	0.054
1.735	1.766	1.842	1.796	1.842	1.594	1.308	1.274
0.005	0.012	0.008	0.009	0.011	0.003	0.007	0.004
0.693	0.494	0.523	0.655	0.469	0.948	1.044	1.059
2.710	2.623	2.676	2.685	2.607	2.704	2.791	2.816
0.015	0.062	0.013	0.013	0.011	0.062	0.112	0.084
0.738	0.684	0.742	0.759	0.723	0.737	0.569	0.563
0.009	0.016	0.011	0.012	0.009	0.010	0.006	0.006
0.762	0.762	0.766	0.784	0.743	0.809	0.687	0.653
0.469	0.521	0.521	0.548	0.583	0.482	0.144	0.130
3.531	3.479	3.479	3.452	3.417	3.518	3.856	3.870
0.71	0.78	0.79	0.73	0.80	0.63	0.56	0.55
0.98	0.92	0.98	0.98	0.99	0.92	0.84	0.87

problems of Al-Mg order-disorder between the Y and Z sites make the assignment of cation site occupancies difficult for Mg-rich tourmalines (Grice and Ercit 1993; Hawthorne et al. 1993).

Analytical results for the Valdeflores tourmalines reveal wide to moderate compositional variations in TiO_2 (0.19–1.24 wt%), CaO (0.02–2.42 wt%), FeO (6.28–13.40 wt%), MgO (1.28–7.78 wt%), Al_2O_3 (29.28–34.48 wt%), and SiO_2 (33.60–38.66 wt%), and smaller variations in Na_2O (1.41–2.66 wt%) and F (0.10–1.34 wt%). Concentrations of MnO are very low (<0.14 wt%). Rb and Cs are below detection limits. ICP analyses of tourmaline concentrates show insignificant amounts of Li (<80 ppm). Boron and H_2O contents have not been determined (Table 1).

On the Al-Fe-Mg and Ca-Fe-Mg ternary discriminant diagrams of Henry and Guidotti (1985), all tourmaline compositions plot within the fields of tourmaline from Li-poor granitoids and metasedimentary rocks (Fig. 4). A progressive increase in Al from the dravite end-member can be observed (Fig. 4b). Estimations from charge balance indicate that Fe^{3+} is negligible in the Valdeflores tourmaline, which is consistent with the lack of data falling below the schorl-dravite join (Fig. 4). The variation from schorl-dravite to olenite-foitite is about 50% of the total range, comparable to the range for most of the tourmaline analyses in terms of Fe-Mg variation. The Fe/(Fe+Mg) ratio increases with Al in the Y-site (Fig. 5a), and the values plot along the line Σ(Fe+Mg) <3 due to Al substitution in the Y-site (Fig. 5b). Negative correlation of Al_{tot} with Si and (Fe+Mg+Mn) is in accordance with the $(Mg,Fe)_{-1}Si_{-1}Al_2$ substitution scheme, and it explains the presence of tetrahedral Al (Figs. 5c and 5d).

All tourmaline has the Al necessary to fill the octahedral Z-site. Apparent Y-site vacancies (Table 1) could be due to the presence of Li, but a plot of Al_Y vs. Y* = Fe + Mg + Mn + Al_Y (Fig. 6a) reveals that the elbaite substitution is negligible, in accordance with the ICP-MS data. Most of the tourmaline compositions fall between the proton- and alkali-deficient exchange vectors (Fig. 6b), which account for the increase of Al content in the Y-site and decrease of X and OH occupancies at the expense of the schorl/dravite end-member. X-site cation totals (Na+Ca+K) vary from 0.64 to 0.9, thus indicating the presence of vacancies in the X-site.

Tourmaline in the Valdeflores area has a limited uvite component with Ca <0.2 atoms per formula unit (apfu). The incorporation of Ca appears to be controlled by one or more of the substitutions: $CaMgNa_{-1}Al_{-1}$, $CaONa_{-1}OH_{-1}$, and $CaMg_2OHNa_{-1}Al_{-2}O_{-1}$ (Fig. 6c). On a

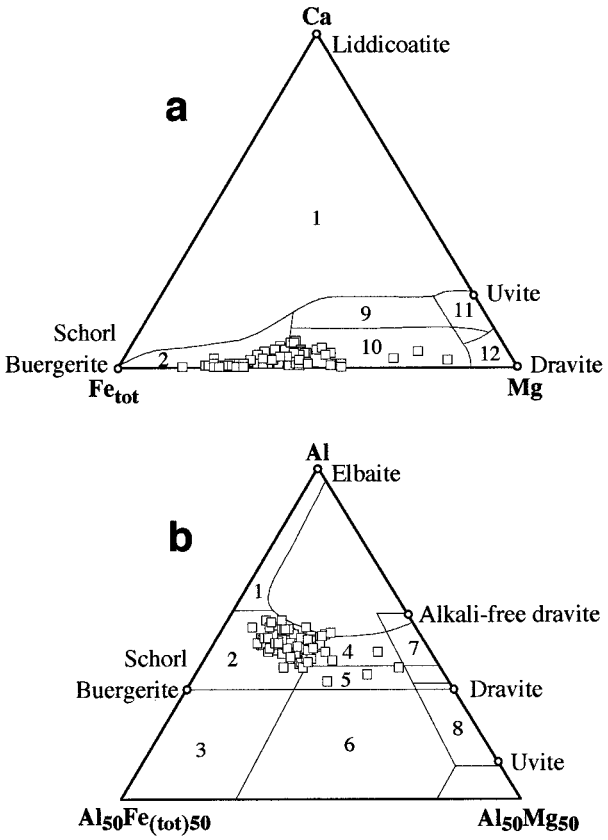

Figure 4. Ternary Fe-Ca-Mg and Fe-Al-Mg diagrams (Henry and Guidotti 1985) showing compositional data for tourmaline from the Valdeflores area. (1) Li-rich granitoid pegmatites and aplites; (2) Li-poor granitoids and associated pegmatites and aplites; (3) Fe^{3+}-rich quartz-tourmaline rocks (hydrothermally altered granites); (4) Metapelites and metapsammites coexisting with an Al-saturating phase; (5) Metapelites and metapsammites not coexisting with an Al-saturating phase; (6) Fe^{3+}-rich quartz-tourmaline rocks, calc-silicate rocks, and metapelites; (7) Low-Ca metaultramafics and Cr, V-rich metasediments; (8) Metacarbonates and meta-pyroxenites; (9) Ca-rich metapelites, metapsammites, calc-silicate rocks; (10) Ca-poor metapelites, metapsammites, and quartz-tourmaline rocks; (11) Metacarbonate rocks; and (12) Metaultramafic rocks.

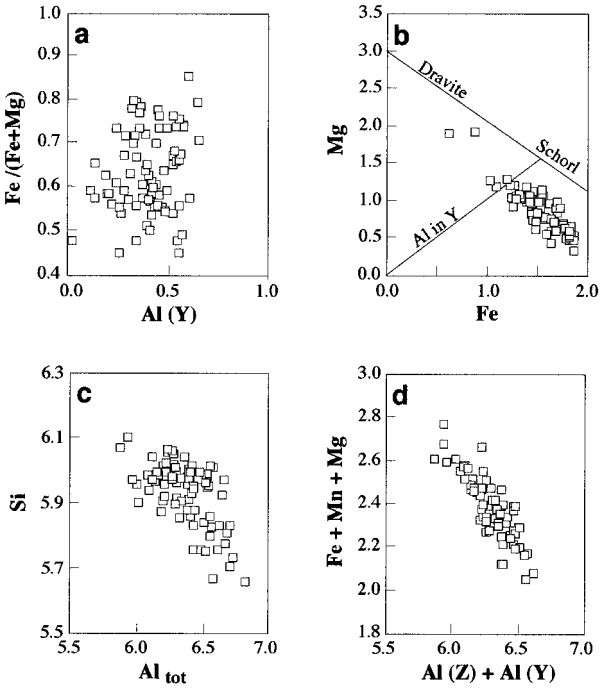

Figure 5. Plots of cation sites occupancies in tourmaline from the Valdeflores area. (**a**) Variation of Al_Y vs. Fe /(Fe+Mg); (**b**) Fe vs. Mg (adapted from London and Manning 1995); schorl-dravite plot along the $\Sigma(Fe+Mg) = 3$, values of $\Sigma(Fe+Mg) < 3$ correspond to Al substitution in Y; (**c**) Al_{tot} vs. Si; (**d**) $Al_Z + Al_Y$ vs. Fe+Mg+Mn.

plot of Na vs. Ca, however, the dispersion of the tourmaline data suggests that other substitutions such as $Ca_{0.5}\square_{0.5}Na_{-1}$ and $\square AlNa_{-1}Mg_{-1}$ may be operative (Fig. 6d). These schemes account for the formation of X-site vacancies.

White mica chemistry

Representative chemical analyses of white micas, together with structural formulae, are reported in Table 2. The proportions of tetrahedral, octahedral, and interlayer cations have been calculated on the basis of 11 O atoms, and the total H_2O as OH^- and interlayer $H_2O°$ were predicted using the model 1 of Loucks (1991). The use of this model for Li-rich micas brings about an excess in the cationic occupancy of the octahedral sites (Table 2). On a plot of $(Mg+Fe+Mn+Ti)/6$ vs. $^{[4]}Al/Al_{tot}$, the Valdeflores white mica compositions lie along a trend from the muscovite end-member toward zinnwaldite (Fig. 7a), suggesting that these micas may have important amounts of Li. This is supported by ICP-MS data of some white mica, which show variable Li_2O contents (up to ≈6.0 wt%; see Table 2) and define a clear positive correlation between F and Li_2O (Fig. 7b). This trend is consistent with the empirical relationships offered by Henderson et al. (1989), Tindle and Webb (1990), and Tischendorf et al. (1997), and demonstrated experimentally in trioctahedral and partly dioctahedral lithium micas by Monier and Robert (1986). On the basis of this positive correlation between Li and F, the Li contents of white micas have been estimated from their F contents determined by electron microprobe.

The chemistry of Valdeflores white mica is characterized by a cation deficiency in the interlayer site [$\Sigma(K+Na+Ca+Cs) \approx 0.61-0.94$ apfu)] and variable amounts of Li, F, and Cs, as well as by the compositional differences between samples from veins and those from tourmalinized metasediments. Representation of the data on a $(Fe_{tot}+Mn+Ti-^{[6]}Al)/(Mg-Li)$ diagram (Tischendorf et al. 1997) indicates that the white mica from tourma-

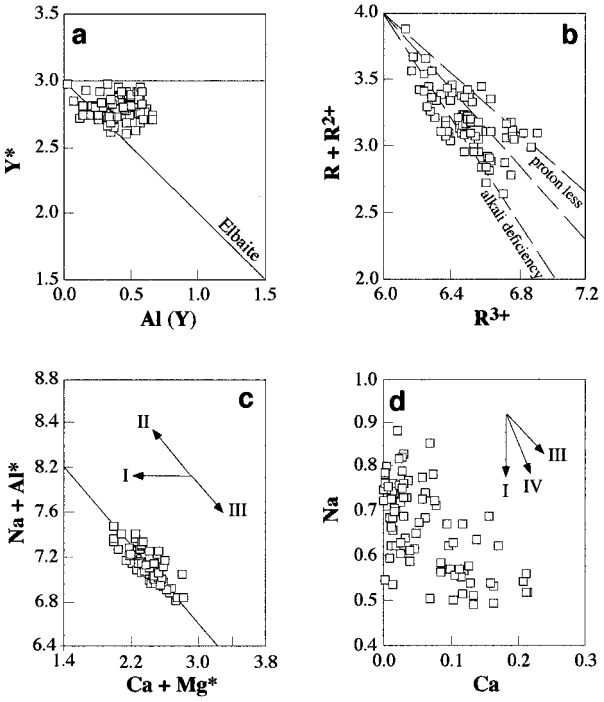

FIGURE 6. Plots of cation sites occupancies of tourmaline from the Valdeflores area. (**a**) occupancy of Y* vs. Al_Y site in apfu (Y* = Fe+Mg+Mn+Al in Y; adapted from London and Manning 1995). Elbaite lies at Y* = Al_Y = 1.5; (B) $R^+ + R^{2+}$ vs. R^{3+} diagram. ($R^+ + R^{2+}$) = ($Na^+ + 2Ca^{2+} + K^+ + Fe^{2+} + Mg^{2+} + Mn^{2+}$) and $R^{3+} = Al^{3+} + 4/3Ti^{4+}$; (C) (Na+Al*) vs. (Ca+Mg*), $Al^* = Al^{3+} + Fe^{3+} + 2Ti - Li$ and $Mg^* = Mg + Fe^{2+} + Mn + 2Li - Ti$ (Henry and Dutrow 1990); (**d**) Na vs. Ca in apfu (I) $\square AlNa_{-1}Mg_{-1}$. (II) $AlOMg_{-1}(OH)_{-1}$. (III) $CaMgNa_{-1}Al_{-1}$, $CaONa_{-1}(OH)_{-1}$, $CaMg_2OHNa_{-1}Al_{-2}O_{-1}$. (IV) $Ca_{0.5}\square_{0.5}Na_{-1}$.

line-rich rocks varies between Li-muscovite, Li-phengite, and lepidolite/zinnwaldite (Figs. 7c and 7d). Lithian muscovite is characterized by the $2M_1$ polytype whereas lepidolite/zinnwaldite micas show the $2M_1$, 1M, and subordinate $2M_2$ polytypes. In general, the white micas have variable F, Al, Fe, and Mg contents ($1.52 \leq F \leq 8.40$ wt%, $20.43 \leq Al_2O_3 \leq 31.20$ wt%, $2.84 \leq FeO_{tot} \leq 10.73$ wt%, and $1.15 \leq MgO \leq 4.55$ wt%). Amounts of Cs_2O are ≤ 1.55 wt%. The variation of F vs. (FeO_{tot}+MgO+MnO), Cs and Al is shown in Figure 8, in which the change of correlation with changing F content is well illustrated. Below about 10 wt% (FeO_{tot}+MgO+MnO), 0.75 wt% Cs_2O, and 22 wt% Al_2O_3 there is a good positive correlation, whereas above these values a negative correlation is observed. Likewise, below 10 wt% FeO_{tot} there is a positive correlation between Li and FeO_{tot}, but above 10 wt% FeO_{tot} the correlation becomes negative (Fig. 8d).

The occurrence of a continuous sequence between lepidolite/zinnwaldite and muscovite is in accordance with the experimental demonstration of solid solution between muscovite and zinnwaldite (Monier and Robert 1986). The incorporation of Li in muscovite may have been developed via the substitution (Mg,Fe)Li $Al_{-1}\square_{-1}$, thus muscovite evolves toward zinnwaldite. By comparison, the micas from veins are mainly dioctahedral in nature and correspond mostly to muscovites and Li-muscovites, characterized by the $2M_1$ polytype (Fig. 7c). They show lower contents of F (1.20–4.23 wt%), Cs (0.16–0.30 wt%), FeO_{tot} (0.89–1.58 wt%), and MgO (0.29–0.90 wt%), but higher contents of Al_2O_3 (29.04–34.61 wt%). These differences are evident graphically on plots of Al, Cs, and (Fe+Mg+Mn) vs. F (Fig. 8).

VIBRATIONAL SPECTROSCOPY OF WHITE MICAS

The presence of Li in the white mica is also supported by FTIR and Raman data. The region of OH-stretching wavenumbers (3700–3400 cm^{-1}) varies depending on the Li and F contents. Representative Raman scattering spectra recorded on micas are presented in Figure 9. The intensity of the high wavenumber OH-stretching band (3627–3624 cm^{-1}) decreases in response to increases in the amount of Li and the extent of F substitution for OH. This may be due to the fact that the Raman intensity is related to the number of oscillators (Gardiner 1989); thus it is consistent with the low hydroxyl content and the predominance of F over OH in the hydroxyl site of Li-rich white mica. Likewise, the OH-stretching bands ($\approx$3629 cm^{-1}) on IR absorption spectra become less intense with the increase of Li and F (Fig. 10). When F replaces OH, it prefers the trioctahedral Li-bearing sites, whereas hydroxyls are adjacent to the vacant octahedral sites. Therefore, OH-stretching bands of lepidolite are the result of dioctahedral hydroxyls and have the same OH-stretching wavenumber as muscovite ($\approx$3629 cm^{-1}) (Robert et al. 1989, 1993). By contrast, the Li-bearing trioctahedral sites are rich in F and reflect no signal in the OH-stretching region (Fig. 10). Two bands at 3435–3430 cm^{-1} and 1640–1630 cm^{-1}, of variable intensity, correspond to molecular H_2O vibrations. A weak band, at 1440–1430 cm^{-1} (Fig. 10) (1450–1425 cm^{-1} Raman), may correspond to the bending (NH_4^+) vibrational mode (Shigorova 1982). Other vibrational bands occur in the range 1200–300 cm^{-1} (Robert et al. 1993), such as the Si-O stretching vibrations between 1120–1000 cm^{-1}, a complex vibration at $\approx$700 cm^{-1} involving both Si-O stretching and O-Si-O bending deformations, and OH-librations and stretching motions in the octahedral layer below 600 cm^{-1} (Fig. 10). A high-wavenumber band grows in the antisymmetric wavenumber range ($\approx$1000 cm^{-1}), both in infrared (1132 cm^{-1}) and in Raman (1142 cm^{-1}) spectra. This is the result of the deviation of mica compositions toward a tetrasilicic trioctahedral mica. This type of band corresponds to the perpendicular T-O vibration in a high-tetrahedral charge mica, i.e., tetrasilicic, and therefore with anisotropic tetrahedra, which explains the band splitting (Robert et al. 1993).

TABLE 2. Representative microprobe analyses of white mica

Rock	V	V	V	V	V	TR	TR
Sample	1	2	3	4	5	6	7
SiO_2	50.12	47.55	48.30	49.07	50.26	48.23	44.96
TiO_2	0.03	0.03	0.05	0.03	0.02	0.25	0.34
Al_2O_3	28.03	36.37	32.96	33.65	29.04	31.20	32.88
FeO_{tot}	1.39	0.42	1.58	0.68	1.58	2.84	2.01
MnO	0.37	0.00	0.04	0.05	0.16	0.09	0.00
MgO	0.17	0.09	0.90	0.17	0.29	1.15	1.30
CaO	0.01	0.01	0.02	0.01	0.00	0.05	0.01
Na_2O	0.29	0.38	0.32	0.37	0.28	0.30	0.44
K_2O	9.80	9.00	8.51	9.53	9.79	8.88	9.48
F	4.81	0.80	1.84	2.02	4.23	2.34	1.98
Cs_2O	0.40	0.14	0.24	0.20	0.30	0.10	0.01
O = F	2.03	0.34	0.77	0.85	1.78	0.98	0.83
Li_2O*	2.34	0.29	0.88	1.00	1.89	1.21	0.97
H_2O*	2.21	5.48	4.50	4.08	2.63	4.07	5.68
Total	99.97	100.56	99.37	100.01	98.69	99.73	100.06
Structural formula on the basis of 11 O atoms							
Si	3.551	3.163	3.273	3.294	3.511	3.297	3.140
$^{[4]}$Al	0.449	0.837	0.727	0.706	0.489	0.703	0.860
(Z)	4.000	4.000	4.000	4.000	4.000	4.000	4.000
$^{[6]}$Al	1.498	1.952	1.762	1.801	1.562	1.627	1.688
Ti	0.002	0.002	0.003	0.002	0.001	0.013	0.018
Fe^{2+}_{tot}	0.082	0.024	0.090	0.039	0.092	0.163	0.118
Mn	0.023	0.000	0.003	0.003	0.010	0.005	0.000
Mg	0.018	0.009	0.092	0.017	0.030	0.117	0.136
Li	0.666	0.079	0.241	0.271	0.531	0.334	0.274
(Y)	2.289	2.066	2.191	2.133	2.226	2.259	2.234
Ca	0.001	0.001	0.001	0.001	0.000	0.004	0.001
Na	0.041	0.049	0.042	0.049	0.038	0.039	0.060
K	0.886	0.764	0.736	0.817	0.873	0.775	0.845
Cs	0.012	0.004	0.007	0.006	0.009	0.003	0.001
(X)	0.940	0.818	0.786	0.873	0.920	0.821	0.907
F	1.078	0.169	0.394	0.430	0.934	0.506	0.438
OH	0.922	1.831	1.606	1.570	1.066	1.494	1.562
$H_2O°$*	0.002	0.184	0.215	0.129	0.080	0.180	0.095
H_3O^+*	–	0.196	–	–	–	–	–
Mg(Mg + Fe)	0.18	0.27	0.51	0.31	0.25	0.42	0.54

* = Calculated; V = mineralized veins; TR = tourmaline-rich rocks.

DARK MICA CHEMISTRY

Electron microprobe analyses (Table 3) show that the dark micas have relatively high contents of Cs_2O (1.14–2.78 wt%) and F (1.60–8.08 wt%), but variable K_2O (5.75–9.04 wt%), and low TiO_2 (<1.20 wt%). Analyses of some samples show up to 0.19 wt% BaO. Amounts of Rb and Cl are below detection limits. FeO contents decrease with increases in Li_2O and F (Fig. 8d). The higher FeO contents correspond to reddish-brown micas, which approach typical biotite compositions and have relatively low F and Cs contents (Figs. 8a and 8b). These compositional differences are consistent with the textural characteristics shown by the mica, and may be used to distinguish between metasomatic and non-metasomatic biotite.

Structural formulae indicate that the tetrahedral positions are filled with Si and Al ($\Sigma^{[4]}Z = 4$). Fe^{3+} has been estimated on the basis of the structural charge neutrality. The total octahedral occupancies vary between 2.57 and 3.21 apfu. The relatively high values are because the number of cations was normalized to yield a total charge of 22. In general, most of the dark mica have values lower than the 3.0 cations in an ideal trioctahedral mica, which illustrates their partial dioctahedral character. Likewise, the abundance of cations in the interlayer $^{[12]}$(K+Na+Ca+Cs) site is deficient (<2.0), ranging from 0.61 to 0.90 apfu (Table 3). The number of OH groups is OH = 2 − F, and H_2O neutral molecules are considered to occupy all interlayer sites that are not occupied by cations, i.e., H_2O. The stoichiometric content of total H_2O as OH^- and interlayer $H_2O°$ has been calculated from the model 1 of Loucks (1991).

The nonideal character of these mica compositions is reflected on the (Mg+Fe+Mn+Ti)/6 vs. $^{[4]}Al/Al_{tot}$ diagram (Fig. 7a). Biotite that deviates from the siderophyllite-annite-phlogopite field shows a trend toward the lepidolite field and falls close to the zinnwaldite end-member, indicating the presence of Li in octahedral sites. Li contents of trioctahedral micas have been estimated from microprobe data using the equation (tri 4b) of Tischendorf et al. (1997). On plots of Fe_{tot}+Mn+Ti-$^{[6]}$Al vs. Mg-Li, the dark mica data show an approximately linear sequence from the compositional field of Mg-Fe mica to Li-Al mica, particularly from Fe-biotite to lepidolite (Fig. 7c). This enrichment in Li is reflected

TABLE 2—*Extended*

TR 8	TR 9	TR 10	TR 11	TR 12	TR 13	TR 14	TR 15
52.60	45.10	47.85	47.45	45.76	49.10	50.13	46.62
0.88	0.85	0.26	0.23	0.50	0.21	0.15	0.09
24.62	20.61	23.17	21.5	21.85	20.94	20.43	22.57
3.30	10.73	7.62	8.60	10.18	7.75	7.02	7.79
0.05	0.10	0.21	0.16	0.17	0.17	0.14	0.09
2.39	4.55	1.60	1.92	1.60	1.81	1.69	2.28
0.02	0.01	0.02	0.01	0.01	0.02	0.01	0.01
0.02	0.07	0.13	0.10	0.10	0.14	0.19	0.09
6.62	8.00	8.83	8.59	8.44	8.41	8.74	6.81
4.54	6.10	6.48	7.22	7.29	8.12	8.04	8.40
0.50	1.29	0.74	0.98	1.01	0.94	0.80	1.55
1.91	2.57	2.73	3.04	3.07	3.42	3.38	3.54
2.12	3.45	3.81	4.54	4.62	5.52	5.42	5.83
3.84	1.82	1.51	1.12	1.05	0.84	0.76	1.14
99.59	100.11	99.50	99.38	99.51	100.55	100.14	99.73
Structural formula on the basis of 11 O atoms							
3.665	3.386	3.525	3.552	3.461	3.629	3.695	3.502
0.335	0.614	0.475	0.448	0.539	0.371	0.305	0.498
4.000	4.000	4.000	4.000	4.000	4.000	4.000	4.000
1.323	0.682	0.987	0.827	0.775	0.762	0.788	0.773
0.046	0.048	0.014	0.013	0.029	0.012	0.008	0.005
0.192	0.674	0.469	0.539	0.644	0.480	0.433	0.489
0.003	0.007	0.014	0.010	0.011	0.011	0.009	0.006
0.248	0.510	0.176	0.214	0.181	0.199	0.186	0.255
0.595	1.043	1.128	1.368	1.401	1.641	1.607	1.762
2.407	2.964	2.788	2.971	3.041	3.105	3.031	3.290
0.002	0.001	0.002	0.001	0.001	0.002	0.001	0.001
0.003	0.011	0.020	0.015	0.015	0.021	0.028	0.013
0.589	0.766	0.830	0.821	0.815	0.793	0.822	0.653
0.015	0.042	0.023	0.031	0.033	0.030	0.025	0.050
0.609	0.820	0.875	0.867	0.864	0.846	0.876	0.717
1.001	1.445	1.510	1.709	1.744	1.899	1.873	1.996
0.999	0.555	0.490	0.291	0.256	0.101	0.127	0.004
0.392	0.181	0.127	0.133	0.138	0.156	0.124	0.285
–	–	–	–	–	–	–	–
0.56	0.43	0.27	0.28	0.22	0.29	0.30	0.34

on the Al-M^{2+}-Si ternary diagram (Fig. 11), in which the biotite compositions move away from the annite-siderophyllite join toward the Li-mica side, becoming progressively more aluminous. Mica that has a relatively high Li content shows a trend toward the polylithionite end-member, consistent with the substitution $(Mg,Fe^{2+})_{-3}Al_{-1}Li_2AlSi$ (Figs. 7c and 11).

As a result of Fe-F avoidance in dark mica solid solutions (e.g., Munoz 1984), the F content of mica by itself is not indicative of the relative enrichment of F in the environment of mica growth. Munoz (1984) defined for this purpose a fluorine intercept (IVF) and index (FI) for biotite. Thus in the case of the Valdeflores area, the (IVF) and (FI) values for Li-poor biotite compositions ranges from 0.90–1.05 and 9.20–8.60, respectively. Application of these data, nevertheless, may be inadequate if relatively high contents of rare alkali elements are present (Munoz and Ludington 1974). Because Valdeflores biotites have low Rb contents and Cs does not correlate with F contents suggests that these elements did not affect substantially the (OH,F) exchange in the biotites. Taking into account that the intercept values or HF activities from biotite analyses depend on the F/(OH) ratio, and the uncertainties relating to anion site occupancy, the estimation of the H_2O content according the model of Loucks (1991) may be a good approximation to obtain reasonable (IVF) values.

DISCUSSION AND CONCLUSIONS

The Li-Sn mineralization in the Valdeflores area is related to emplacement and consolidation of the Cabeza de Araya batholith (Santos and Medina 1978). Based on geological and mineralogical evidence, however, Torres-Ruiz et al. (1996) presented a model in which a small granitic stock at depth was responsible for producing the B-F-Li and Cs metasomatism and mineralized veins. In general, the granites of the Cáceres region are characterized by relatively high contents of K, Li, Rb, Sn, F, B, P, and U (Bea 1976; Corretgé et al. 1985; Pérez del Villar 1988). The veins may have acted as channels for the ascending granite-derived hydrothermal fluids rich in B, F, P, rare alkalis, and Sn. Cassiterite precipitated in the veins, accompanied by a variable mineral assemblage including quartz, Li-mica, amblygonite-montebrasite (X_{amb} = 0.2), Sr-rich fluorapatite (up to 8.7 wt% SrO), fluorite, topaz (X_F = 0.9), and locally potassium feldspar. Petrographic and mineralogical data suggest that hydrothermal fluids rich in B-Li-F and Cs, previously concentrated dur-

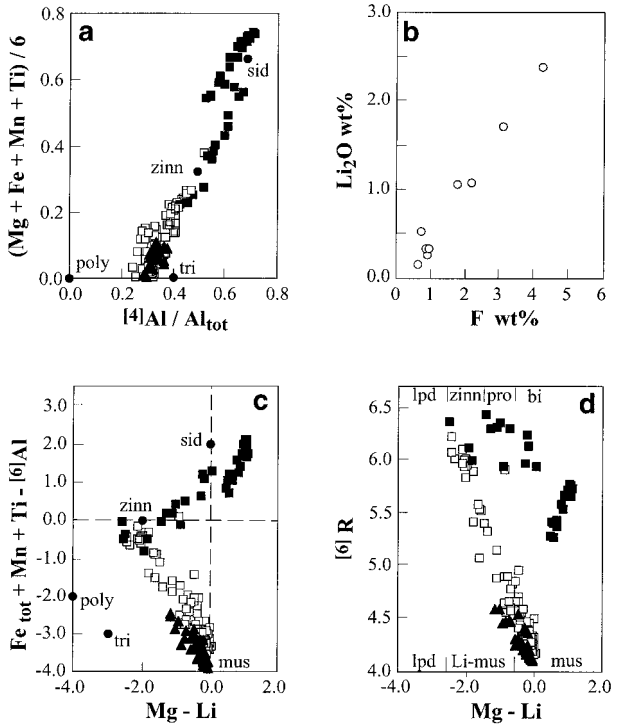

FIGURE 7. (**a**) $^{[4]}Al/Al_{tot}$ vs. (Mg+Fe+Mn+Ti)/6 for mica from the Valdeflores area. (**b**) Variation of Li_2O vs. F for white mica. (**c**) Position of the Valdeflores mica in the (Fe_{tot}+Mn+Ti-$^{[6]}$Al)/(Mg-Li) diagram (Tischendorf et al. 1997). (**d**) Compositions of Valdeflores mica in terms of (Mg-Li) and octahedral occupancy ($^{[6]}$R). bi = biotite solid solution; Li-mus = Li muscovite; lpd = lepidolite; mus = muscovite; poly = polylithionite; pro = protolithionite; sid = siderophyllite; tri = trilithionite; zinn = zinnwaldite. Black squares = dark mica; open squares = white mica; triangles = vein mica.

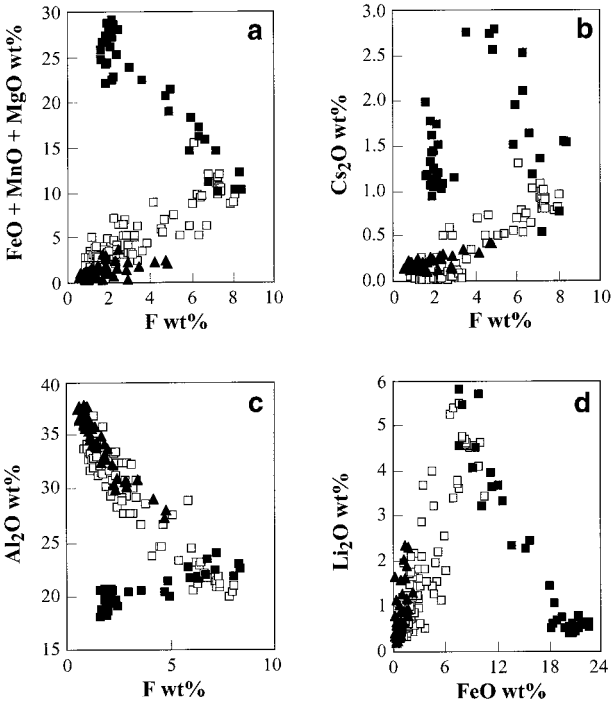

FIGURE 8. Plot of Valdeflores mica compositions. (**a**) F vs. FeO+MgO+MnO; (**b**) F vs. Cs_2O; (**c**) F vs. Al_2O_3; and (**d**) FeO vs. Li_2O. Symbols as in Figure 7.

ing magmatic evolution, reacted with pelitic metasediments to form tourmaline, Li-F-Cs micas, and topaz.

Tourmalinization, Li-F-Cs metasomatism, and vein formation

The spatial distribution of the veins and the extensive associated B-Li-F-Cs metasomatism in the Valdeflores area suggest that the mineralized veins and tourmalinization are related to fluids derived from the same granitic source in a tectonically active regime. Experimental work shows that B, F, and P lower the liquidus and solidus temperatures, and the combined effects of these elements enhance the solubilities of H_2O and control the behavior of incompatible lithophile elements (London 1987; Manning and Pichavant 1988; Dingwell 1988; Webster and Holloway 1990; London et al. 1996; Dingwell et al. 1996). The solidus depression and enhancement of H_2O miscibility may give rise to a supercritical fluid from magmatic to hydrothermal conditions. In this way, shearing processes that affected the Valdeflores area may have changed the evolution of the system by breaking down its physical-chemical continuity, and triggering the abrupt transition from closed- to open-system behavior. If the system contains insufficient Fe and Mg to conserve all boron as tourmaline, most of the boron will be lost to wallrocks with subsequent formation of tourmaline (Wolf and London 1997).

The low concentrations of F, Li, and Cs in the Valdeflores tourmaline may reflect genuine partitioning more

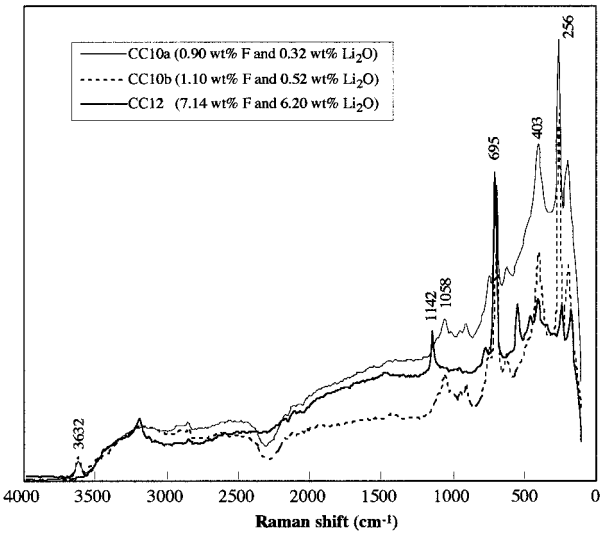

FIGURE 9. Raman spectra of white mica from the Valdeflores area with variable Li and F contents.

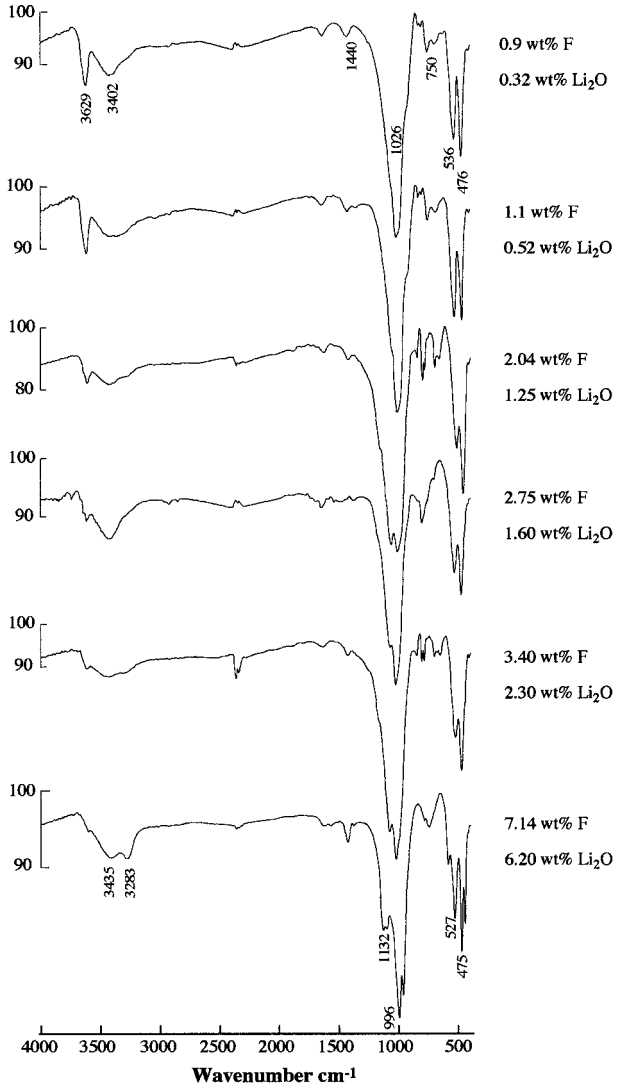

FIGURE 10. FTIR spectra of white mica from the Valdeflores area with variable Li and F contents.

than sequential metasomatism in which the influx of Li-F-Cs-rich fluids occurred during tourmaline crystallization. Petrographic observations do not reveal a temporal sequence between tourmaline and the micas. Although boron shows a preference for the vapor ($K^{vapor/melt} > 1$: Pichavant 1981; London et al. 1988), so that the system would fractionate boron from other elements, the B and Li-F-Cs metasomatic events appear to have been juxtaposed. Differences in cation field strength are important in controlling the fractionation processes and cation substitutions, and the Fe-Mg contents in the host rocks were high enough to stabilize Fe-Mg tourmaline. Subsequently, Li and other alkalis were distributed into coexisting micas.

If most of the fluids were channeled through fractures, the lack of tourmaline in the veins is believed to be the result of the alkalinity and low Fe-Mg contents of the fluids. B, F, and P promote the concentration of Sn and other high field strength elements, which tend to increase the alkalinity of the system (London et al. 1989). As tourmaline is unstable in fluids with pH > 6.5 and in systems having very low Fe-Mg contents, the boron would be expelled into host rocks yielding external tourmalinization (Morgan and London 1989). Although tourmaline shows a relatively large compositional range, no systematic variations with distance from veins has been observed. However, the mineral association varies in such a manner that topaz and arsenopyrite are located near the veins. In addition to boron, other excess components such as F, Li, and Cs would be transported via an exsolved fluid phase. These elements show similar trends suggesting that they existed within the same metasomatic fluid (Figs. 7b and 8b). The distribution of cassiterite in the veins may be due to the partitioning of Sn between a fluid phase and silicate melt, because fluorine and other volatiles increase the efficiency of metal scavenging by the fluid phase.

Compositional evolution of the micas

The partitioning of Li, Cs, and F into biotite over muscovite has been documented in several studies (e.g., Volfinger 1976; Volfinger and Robert 1980; Wilson and Long 1983; Dahl et al. 1993; Icenhower and London 1995; Neves 1997). Neves (1997) gives average partition ratios ($D^{Bt/Ms} \pm 1\sigma$) for Li, Cs, and F of 4.0 ± 2.1, 4.3 ± 1.3, and 1.8 ± 0.5, respectively. However, the white mica of Valdeflores shows higher F and Li contents than coexisting dark mica. This is the consequence of their compositional evolution during metasomatism as well as the miscibility gap between Li-free trioctahedral and dioctahedral micas, which decreases with increasing Li content (Monier and Robert 1986). Biotite and muscovite compositions become progressively closer with increasing Li content, so that for high Li concentrations a single mica crystallizes. This would explain the observation that the dark mica and white mica show convergent trends with increasing F and FeO contents (Figs. 8a, 8b, and 8d). During metasomatic processes biotite can evolve compositionally toward polylithionite via the substitution $(Mg,Fe)_{-3}Al_{-1}Li_2AlSi$. Thus, biotite in the tourmaline-rich rocks of the Valdeflores area may represent a relict feature as a result of disequilibrium processes during metasomatism. Muscovite can acquire a trioctahedral character of zinnwaldite by the substitution $Al_{-1}\square_{-1}(Fe^{2+},Mg)Li$, thus explaining the relatively high Fe contents of many white mica grains in the tourmalinites. However, despite the appearance of a continuous sequence between zinnwaldite and muscovite in the $(Fe_{tot}+Mn+Ti-^{[6]}Al)/(Mg-Li)$ diagram (Fig. 7c), there is no clear evidence that compositions migrate along the muscovite-zinnwaldite join in the M^{2+}-Al-Si diagram (Fig. 11). The dispersion of data that appears in this figure between the muscovite-zinnwaldite join and the Li-Al side suggests that other mechanisms, such as the substitutions $SiLi_2Al_{-2}\square_{-1}$ and $Li_3Al_{-1}\square_{-2}$, also may have operated to incorporate Li into

TABLE 3. Representative microprobe analyses of dark mica

Sample	1	2	3	4	5	6	7
SiO_2	45.16	42.90	40.17	40.42	42.48	43.33	46.18
TiO_2	0.27	1.11	0.65	0.70	0.54	0.28	0.28
Al_2O_3	27.60	22.82	21.80	21.84	22.23	22.47	21.84
FeO_{tot}	5.91	10.36	12.85	12.22	11.45	9.68	8.14
MnO	0.05	0.10	0.11	0.12	0.13	0.10	0.09
MgO	1.40	4.13	5.29	4.87	4.23	4.80	1.86
CaO	0.01	0.01	0.00	0.00	0.03	0.00	0.01
Na_2O	0.22	0.15	0.16	0.10	0.26	0.17	0.13
K_2O	9.04	7.50	7.51	7.40	7.58	7.97	8.48
F	5.09	5.84	5.98	6.34	6.66	7.19	8.08
Cs_2O	0.50	1.52	1.94	2.11	1.64	1.35	0.75
O = F	2.15	2.46	2.52	2.67	2.80	3.03	3.40
Li_2O*	2.57	3.21	3.34	3.67	3.98	4.51	5.47
H_2O*	2.10	1.99	1.65	1.51	1.43	1.20	0.66
Total	97.77	99.18	98.93	98.63	99.84	100.02	98.57
Structural formula on the basis of 11 O atoms							
Si	3.317	3.250	3.130	3.160	3.245	3.279	3.504
$^{[4]}Al$	0.683	0.750	0.870	0.840	0.755	0.721	0.496
(Z)	4.000	4.000	4.000	4.000	4.000	4.000	4.000
$^{[6]}Al$	1.275	0.778	0.595	0.602	0.661	0.657	0.752
Ti	0.015	0.064	0.038	0.042	0.031	0.016	0.016
Fe^{3+}	–	–	–	–	–	–	–
Fe^{2+}	0.363	0.656	0.837	0.799	0.731	0.613	0.517
Mn	0.003	0.007	0.008	0.008	0.009	0.007	0.006
Mg	0.153	0.467	0.615	0.568	0.482	0.541	0.211
Li	0.758	0.979	1.046	1.154	1.223	1.373	1.668
(Y)	2.567	2.951	3.139	3.173	3.137	3.207	3.170
Ca	0.001	0.001	0.000	0.000	0.003	0.000	0.001
Na	0.032	0.023	0.024	0.016	0.039	0.025	0.019
K	0.848	0.745	0.747	0.739	0.738	0.770	0.821
Cs	0.016	0.049	0.065	0.071	0.054	0.044	0.024
(X)	0.897	0.798	0.835	0.826	0.834	0.839	0.865
F	1.183	1.400	1.474	1.566	1.609	1.720	1.938
OH	0.187	0.600	0.526	0.434	0.391	0.280	0.062
H_2O°*	0.105	0.204	0.166	0.176	0.168	0.162	0.135
Mg/(Mg + Fe)	0.30	0.42	0.42	0.42	0.40	0.47	0.29

* = Calculated.

the octahedral sheet of muscovite. The incorporation of the polylithionite component in white mica solid solutions is supported by the spectroscopic data (Figs. 9 and 10). Consequently, it is probable that a significant proportion of Fe-rich white mica originally was biotite.

The cation deficiency in the interlayer site of micas is believed to correspond to an excess of (F+OH) in the unit cell (Levillain 1980). The commonly inferred occurrence of interlayer vacancies is virtually nonexistent because the supposed vacancies are occupied by hydronium ions and H_2O molecules. The occurrence of H_2O molecules is supported by thermogravimetric and spectroscopic data, and estimations of the H_2O content using the models of Loucks (1991) are in accord with the analytical results. Some mica samples with low Li contents show H_2O in interlayer sites as a combination of H_2O and H_3O^+ (Table 2). The hydronium ion is believed to be a substantial interlayer site occupant in white mica formed in acidic to neutral pH environments at temperatures below ≈450 °C (Loucks 1991). These conditions are consistent with the metasomatic processes that developed in the Valdeflores area.

Interpretation of fluorine intercept data

The high fluorine indices and relatively low log (f_{H_2O}/f_{HF}) ratios denote F-rich micas and a high fluorine content of the hydrothermal fluids. Taking into account the geothermometry based on partitioning of Mg and Fe between tourmaline and biotite (Henry and Dutrow 1996), for tourmaline-biotite partitioning data from Valdeflores we can assume a reasonable temperature regime of (400 °C. Thus the log (f_{H_2O}/f_{HF}) values (calculated after Munoz 1984) for the fluids in equilibrium with Li-poor biotite are 4.02–4.17. Log (f_{H_2O}/f_{HF}) values determined from the topaz F-OH exchange reaction (Barton 1982) for the fluids in equilibrium with topaz (average $X_F \approx 0.8$) in the tourmaline-rich rocks are in the range 4.30–4.60 approximately. The magmatic-hydrothermal link of the fluorine is shown by the occurrence of amblygonite-montebrasite, fluorapatite, fluorite, topaz, and F-bearing mica in the veins. Log (f_{H_2O}/f_{HF}) values calculated for the fluids in equilibrium with amblygonite-montebrasite (average $X_{amb} = 0.20$), based on the method of Loh and Wise (1976), are 6.4–6.7, which are greater than the values calculated for fluids in equilibrium with Li-poor biotite and topaz.

TABLE 3—*Extended*

8	9	10	11	12	13	14	15
39.35	36.06	35.49	36.27	36.35	36.84	36.07	35.85
0.32	0.34	1.00	0.26	0.85	0.33	0.26	0.48
20.37	19.56	18.67	19.78	19.36	20.70	20.00	19.42
18.68	22.69	22.44	22.73	22.56	21.91	22.33	22.72
0.11	0.08	0.12	0.09	0.12	0.12	0.10	0.10
5.14	6.03	5.92	6.22	5.91	5.17	5.45	6.02
0.02	0.02	0.04	0.06	0.02	0.03	0.02	0.01
0.09	0.12	0.25	0.08	0.05	0.06	0.14	0.11
6.31	5.90	5.75	5.89	5.80	6.57	6.23	5.77
2.97	1.97	1.99	2.16	2.20	2.15	2.02	1.94
1.13	1.23	1.45	1.14	1.20	1.20	1.04	1.42
1.25	0.83	0.84	0.91	0.93	0.91	0.85	0.82
1.06	0.54	0.55	0.63	0.64	0.62	0.56	0.52
4.14	4.24	4.42	4.44	4.24	4.24	4.26	4.43
98.44	98.12	97.07	98.82	98.57	99.03	97.63	97.97
Structural formula on the basis of 11 O atoms							
2.890	2.762	2.755	2.750	2.762	2.773	2.766	2.757
1.110	1.238	1.245	1.250	1.238	1.227	1.234	1.243
4.000	4.000	4.000	4.000	4.000	4.000	4.000	4.000
0.654	0.528	0.463	0.518	0.496	0.610	0.574	0.517
0.018	0.020	0.059	0.015	0.049	0.019	0.015	0.028
0.691	0.479	0.490	0.519	0.530	0.514	0.491	0.473
0.457	0.975	0.967	0.923	0.904	0.866	0.942	0.989
0.007	0.006	0.008	0.006	0.008	0.008	0.007	0.007
0.563	0.689	0.685	0.703	0.670	0.581	0.623	0.691
0.312	0.166	0.171	0.191	0.197	0.189	0.173	0.162
2.702	2.863	2.843	2.875	2.854	2.787	2.825	2.867
0.001	0.002	0.004	0.005	0.002	0.003	0.002	0.001
0.013	0.018	0.038	0.012	0.008	0.009	0.021	0.017
0.592	0.577	0.570	0.570	0.562	0.631	0.610	0.566
0.036	0.040	0.048	0.037	0.039	0.039	0.034	0.047
0.642	0.637	0.660	0.624	0.611	0.682	0.667	0.631
0.689	0.477	0.488	0.518	0.528	0.512	0.489	0.471
1.311	1.523	1.512	1.482	1.472	1.488	1.511	1.529
0.360	0.364	0.342	0.377	0.390	0.320	0.335	0.371
0.33	0.32	0.32	0.33	0.32	0.30	0.30	0.32

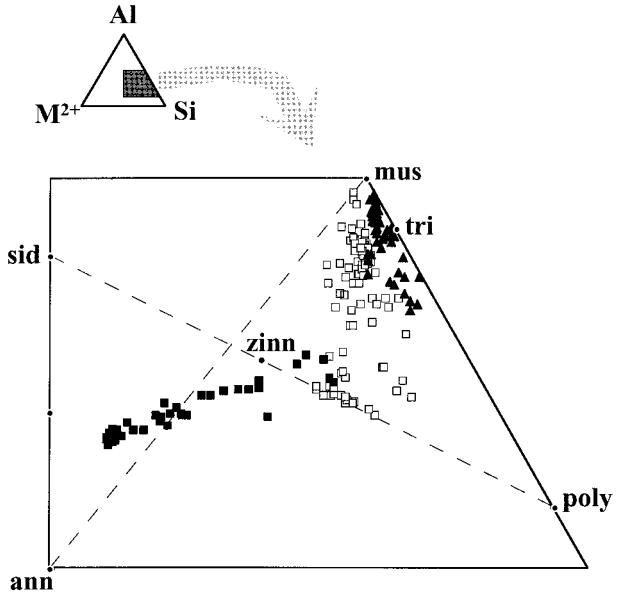

FIGURE 11. Plot of mica compositions in the M^{2+}-Al-Si diagram. Abbreviations and symbols as Figure 7; ann = annite.

As Munoz (1984) argued, the differences of the log (f_{H_2O}/f_{HF}) values may be due to the relative f_{HF} that prevailed during F = OH exchange or to differences in temperature. In the case of Valdeflores there are no direct geothermometric data, but it is probable that these differences reflect the existence of gradients in relative f_{HF} more than temperature variations between veins and host rocks. The difference in log (f_{H_2O}/f_{HF}) could be diminished if the amblygonite-montebrasite exchanged F at higher temperatures than the biotite in the tourmalinites. A difference of ≈500 °C between exchange temperatures, however, is required to make the fugacity ratios similar (temperatures of ≈900 °C in the veins). Therefore, differences in log (f_{H_2O}/f_{HF}) appear to reflect a significant difference in the relative f_{HF} between the veins and tourmaline-rich rocks.

ACKNOWLEDGMENTS

We are grateful to J.-L. Robert and J.F. Slack for helpful comments and suggestions that improved this paper. We also thank D. London and L. Groat for constructive reviews. This study has been carried out with the financial support of the Spanish CICYT (project no. PB 95/350).

REFERENCES CITED

Bailey, S.W. (1984) Appendix. X-ray identification of mica polytypes. In Mineralogical Society of America Reviews in Mineralogy, 13, 573–584.

Barton, M.D. (1982) The thermodynamic properties of topaz solid solutions and some petrologic applications. American Mineralogist, 67, 956–974.

Bea, F. (1976) Anomalía geoquímica de los granitoides calcoalcalinos hercínicos del área Cáceres-Salamanca-Zamora (España). Implicaciones petrogenéticas. Studia Geologica, XI, 25–73.

Cěrný, P. and Burt, D.M. (1984) Paragenesis, crystallochemical characteristics, and geochemical evolution of micas in granite pegmatites. In Mineralogical Society of America Reviews in Mineralogy, 13, 257–297.

Corretgé, L.G., Bea, F., and Suarez, O. (1985) Las características geoquímicas del batolito de Cabeza de Araya (Cáceres, Espana): Implicaciones petrogenéticas. Trabajos de Geología, 15, 219–238.

Dahl, P.S., Wehn, D.C., and Feldmann, S.G. (1993) The systematics of trace-element partitioning between coexisting muscovite and biotite in metamorphic rocks from the Black Hills, South Dakota, USA. Geochimica et Cosmochimica Acta, 57, 2487–2505.

Dingwell, D.B. (1988) The structures and properties of fluorine-rich magmas, A review of experimental studies. In Taylor R.P. and Strong D.F., Eds., Recent advances in the geology of granite-related mineral deposits. Canadian Institution of Mining and Metallurgy, Special vol. 39, 1–12.

Dingwell, D.B., Pichavant, M., and Holtz, F. (1996) Experimental studies of boron in granitic melts. In Mineralogical Society of America Reviews in Mineralogy, 33, 331–385.

Finch, A.A., Parsons, I., and Mingard, S.C. (1995) Biotites as indicators of fluorine fugacities in late-stage magmatic fluids: The Gardar Province of South Greenland. Journal of Petrology, 36, 1701–1728.

Foord, E.E., Cěrný, P., Jackson, L.L., Sherman, D.M., and Eby, R.K. (1995) Mineralogical and geochemical evolution of micas from miarolitic pegmatites of the anorogenic Pikes Peak batholith, Colorado. Mineralogy and Petrology, 55, 1–26.

Gallagher, V. and Kennan, P.S. (1992) Tourmaline on the margin of the Leinster Granite, southeast Ireland: Petrogenetic implications. Irish Journal Earth Sciences, 11, 131–150.

Gardiner, D.J. (1989) Introduction to Raman scattering. In D.J. Gardiner and P.R. Graves, Eds., Practical Raman spectroscopy, 157 p. Springer Verlag, Berlin.

Glebov, M.P., Glyuk, D.S., Sobachenko, V.N., and Shmakin, B.M. (1974) Geochemistry of formation of cesium mica aggregates in amphibolites. Geochemistry International, 9, 937–943.

Grice, J.D. and Ercit, T.S. (1993) Ordering of Fe and Mg in the tourmaline crystal structure: The correct formula. Neues Jahrbuch für Mineralogie Abhandlungen, 165, 245–266.

Hawthorne, F.C. (1996) Structural mechanisms for light-element variations in tourmaline. Canadian Mineralogist, 34, 123–132.

Hawthorne, F.C., MacDonald, D.J., and Burns, P.C. (1993) Reassignment of cation site occupancies in tourmaline: Al-Mg disorder in the crystal structure of dravite. American Mineralogist, 78, 265–270.

Hecht, L. (1994) The chemical composition of biotite as an indicator of magmatic fractionation and metasomatism in Sn-specialised granites of the Fichtelgebirge (NW Bohemian Massif, Germany). In Seltmann, Kämpf and Möller, Eds., Metallogeny of Collisional Orogens, Czech Geological Survey, Prague, 295–300.

Henderson, C.M.B., Martin, J.S., and Mason, R.A. (1989) Compositional relations in Li-micas from S.W. England and France: an ion- and electron-microprobe study. Mineralogical Magazine, 53, 427–449.

Henry, D.J. and Guidotti, C.V. (1985) Tourmaline as a petrogenetic indicator mineral: An example from the staurolite-grade metapelites of NW Maine. American Mineralogist, 70, 1–15.

Henry, D.J. and Dutrow, B.L. (1990) Ca substitution in Li-poor aluminous tourmaline. Canadian Mineralogist, 28, 101–114.

———(1996) Metamorphic tourmaline and its petrologic applications. In Mineralogical Society of America Reviews in Mineralogy, 33, 503–557.

Icenhower, J. and London, D. (1995) An experimental study of element partitioning among biotite, muscovite, and coexisting peraluminous silicic melt at 200 MPa (H_2O). American Mineralogist, 80, 1229–1251.

Jollif, B.L., Papike, J.J., and Shearer, C.K. (1986) Tourmaline as a recorder of pegmatite evolution: Bob Ingersoll pegmatite, Black Hills, South Dakota. American Mineralogist, 71, 472–500.

———(1987) Fractionation trends in mica and tourmaline as indicators of pegmatite internal evolution: Bob Ingersoll pegmatite, Black Hills, South Dakota. Geochimica et Cosmochimica Acta, 51, 519–534.

Lentz, D. (1992) Petrogenesis and geochemical composition of biotites in rare-element granitic pegmatites in the southwestern Grenville Province, Canada. Mineralogy and Petrology, 46, 239–256.

Levillain, C. (1980) Etude statistique des variations de la teneur en OH et F dans les micas. TMPM Tschermaks Mineralogische und Petrographische Mitteilungen, 27, 209–223.

Loh, S.E. and Wise, W.S. (1976) Synthesis and fluorine-hydroxyl exchange in the amblygonite series. Canadian Mineralogist, 14, 357–363.

London, D. (1987) Internal differentiation of rare-element pegmatites: Effects of boron, phosphorous, and fluorine. Geochimica et Cosmochimica Acta, 51, 403–420.

London, D. and Manning, D.A.C. (1995) Chemical variation and significance of tourmaline from southwest England. Economic Geology, 90, 495–519.

London, D., Hervig, R.L., and Morgan, G.B. VI (1988) Melt-vapor solubilities and elemental partitioning in peraluminous granite-pegmatite systems: Experimental results with Macussani glass at 200 MPa. Contribution to Mineralogy and Petrology, 99, 360–373.

London, D., Morgan, G.B. VI, and Hervig, R.L. (1989) Vapor-undersaturated experiments with Macusani glass + H_2O at 200 MPa, and the internal differentiation of granitic pegmatites. Contribution to Mineralogy and Petrology, 102, 1–17.

London, D., Morgan, G.B. VI, and Wolf, M.B. (1996) Boron in granitic rocks and their contact aureoles. In Mineralogical Society of America Reviews in Mineralogy, 33, 299–330.

López Plaza, M. and Martínez Catalán, J.R. (1988) Síntesis estructural de los granitoides del Macizo Hespérico. In F. Bea, A. Carnicero, J.C. Gonzalo, M. López Plaza, M.D. Rodriguez Alonso, Eds., Geología de los granitoides y rocas asociadas del Macizo Hespérico. Editorial Rueda, Madrid, 195–210.

Loucks, R.R. (1991) The bound interlayer H_2O content of potassic white micas: Muscovite-hydromuscovite-hydropyrophyllite solutions. American Mineralogist, 76, 1563–1579.

Manning, D.A.C. and Pichavant, M. (1988) Volatiles and their bearing on the behaviour of metals in granitic systems. In R.P. Taylor and D.F. Strong, Eds., Recent advances in the geology of granite-related mineral deposits. Canadian Institution of Mining and Metallurgy. Special vol. 39, 13–24.

Monier, G. and Robert, J.-L. (1986) Evolution of the miscibility gap between muscovite and biotite solid solutions with increasing lithium content: an experimental study in the system K_2O-Li_2O-MgO-FeO-Al_2O_3-SiO_2-H_2O-HF at 600°C, 2 kbar P_{H_2O}: comparison with natural lithium micas. Mineralogical Magazine, 50, 641–651.

Morgan, G.B.VI and London, D. (1987) Alteration of amphibolitic wallrocks around the Tanco rare-element pegmatite, Bernic Lake, Manitoba. American Mineralogist, 72, 1097–1121.

———(1989) Experimental reactions of amphibolite with boron-bearing aqueous fluids at 200MPa: Implications for tourmaline stability and partial melting in mafic rocks. Contribution to Mineralogy and Petrology, 102, 281–297.

Munoz, J.L. (1984) F-OH and Cl-OH exchange in micas with applications to hydrothermal ore deposits. In Mineralogical Society of America Reviews in Mineralogy, 13, 469–493.

Munoz, J.L. and Ludington, S.D. (1974) Fluorine-hydroxyl exchange in biotite. American Journal of Sciences, 274, 396–413.

Neves, L.J.P.F. (1997) Trace element content and partitioning between biotite and muscovite of granitic rocks: A study in the Viseu region (Central Portugal). European Journal of Mineralogy, 9, 849–857.

Pérez del Villar, L. (1988) El uranio en el batolito de Cabeza de Araya y en el C.E.G. del borde septentrional (Cáceres): Prospección, geoquímica, mineralogía y metalogenia, 470 p. Thesis, Universidad de Salamanca.

Pichavant, M. (1981) An experimental study of the effect of boron on a water saturated haplogranite at 1 kbar vapour pressure. Contribution to Mineralogy and Petrology, 76, 430–439.

Pouchou, J.L. and Pichoir, F. (1985) ''PAP'' (f) (r) (t) procedure for improved quantitative microanalisis. In J.T. Armstrong, Ed., Microbean Analysis, 104 p. San Francisco Press, San Francisco, California.

Robert, J.-L., Bény, J.-M., Beny, C., and Volfinger, M. (1989) Characterization of lepidolites by Raman and Infrared spectrometries. I. Relationships between OH-stretching wavenumbers and composition. Canadian Mineralogist, 27, 225–235.

Robert, J.-L., Bény, J.-M., Della Ventura, G., and Hardy, M. (1993) Fluorine in micas: crystal-chemical control of the OH-F distribution between trioctahedral and dioctahedral sites. European Journal of Mineralogy, 5, 7–18.

Roda, E., Pesquera, A., and Velasco, F. (1995) Micas of the muscovite-lepidolite series from the Fregeneda pegmatites (Salamanca, Spain). Mineralogy and Petrology, 55, 145–157.

Santos, J.A. and Medina, E. (1978) Emplazamiento geológico y características de los filones mineralizados en ambligonita-casiterita de Valdeflores (Cáceres). Tecniterrae, 21, 32–38.

Shigorova, T.A. (1982) The possibility of determining the ammonium content of mica by IR spectrometry. Geochemistry International, 19, 110–114.

Slack, J.F. (1996) Tourmaline associations with hydrothermal ore deposits. In Mineralogical Society of America Reviews in Mineralogy, 33, 559–643.

Stone, M., Klomínsky, J., and Rajpoot, G.S. (1997) Composition of trioctahedral micas in the Karlovy Vary pluton, Czech Republic and a comparison with those in the Cornubian batholith, SW England. Mineralogical Magazine, 61, 791–807.

Tindle, A.G. and Webb, P.C. (1990) Estimation of lithium contents in trioctahedral micas using microprobe data: application to micas from granitic rocks. European Journal of Mineralogy, 2, 595–610.

Tischendorf, G., Gottesmann, B, Förster, H.-J., and Trumbull, R.B. (1997) On Li-bearing micas: estimating Li from electron microprobe analyses and an improved diagram for graphical representation. Mineralogical Magazine, 61, 809–834.

Torres-Ruiz, J., Pesquera, A., Gil Crespo, P.P., and Casas, J. (1996) Tourmalinites and Sn-Li mineralization in the Valdeflores area (Cáceres, Spain). Mineralogy and Petrology, 56, 209–223.

van Middelaar, W.T. and Keith, J.D. (1990) Mica chemistry as an indicator of oxygen and halogen fugacities in the Can tung and other W-related granitoids in the North American Cordillera. In H.J. Stein and J.L. Hannah, Eds., Ore-bearing granite systems; petrogenesis and mineralizing processes. Geological Society of America, Special Paper, 246, 205–220.

Volfinger, M. (1976) Effet de la température sur les distributions de Na, Rb et Cs entre la sanidine, la muscovite, la phlogopite et une solution hydrothermale sous une pression de 1 kb. Geochimica et Cosmochimica Acta, 40, 267–282.

Volfinger, M. and Robert, J.-L. (1980) Structural control of the distribution of trace elements between silicates and hydrothermal solutions. Geochimica et Cosmochimica Acta, 44, 1455–1461.

Webster, J.D. and Holloway, J.R. (1990) Partitioning of F and Cl between magmatic hydrothermal fluids and highly evolved granitic magmas. In H.J. Stein and J.L. Hannah, Eds., Ore-bearing granite systems; petrogenesis and mineralizing processes. Geological Society of America, Special Paper, 246, 21–34.

Wilson, G.C. and Long, J.V.P. (1983) The distribution of lithium in some Cornish minerals: ion microprobe measurements. Mineralogical Magazine, 47, 191–199.

Wolf, M.B. and London, D. (1997) Boron in granitic magmas: stability of tourmaline in equilibrium with biotite and cordierite. Contribution to Mineralogy and Petrology, 130, 12–30.

Manuscript received April 8, 1998
Manuscript accepted August 11, 1998
Paper handled by David London